

Effect of Mechanical Aortic Valves on Coronary Artery Flow in a Patient Suffering from Ischemic Heart Disease



Anna Nieroda, Krzysztof Jankowski, and Marek Pawlikowski

Abstract Coronary artery disease is the most common cardiovascular condition and one of the leading causes of death worldwide. Coronary artery disease is caused by a narrowing or complete occlusion of the coronary artery lumen. Early diagnosis and correct assessment of the existing stenosis are essential. In our study, a pilot study in this regard, we present a method of non-invasive FFR estimation based on 3D numerical simulations of blood flow through coronary arteries in a 50-year-old man with coronary artery stenosis. Our study considered patient-specific coronary artery geometry. The study determined the effect of blood pressure gradient in flow across mechanical trileaflet (TRI) and bileaflet (BIL) and natural aortic valves on the fractional coronary flow reserve (FFR) value. The predicted value of the FFR ratio for the natural valve is 82% while the FFR value from coronarography is 83%. The predicted FFR values for BIL and TRI mechanical valves are 77% and 75%, respectively.

Keywords Aortic valve · Mechanical valve · Coronary artery · Blood flow · FFR

1 Introduction

One of the most common diseases of the cardiac system is ischemic heart disease (IHD) also called coronary heart disease (CHD). It still remains the main cause of mortality in the world [1, 2]. Patients suffering from IHD are treated either conservatively by means of medications [3] or invasively by means of percutaneous revascularization [4] or coronary artery bypass surgery [5]. An invasive intervention must be preceded by an accurate examination of patients which will give a clear indication of whether or not they may be qualified for a surgical procedure. To detect ischemia caused by artery stenosis fractional flow reserve (FFR) ratio is commonly measured [6–8]. FFR, which is the gold standard for diagnosis of the functional

A. Nieroda · K. Jankowski · M. Pawlikowski (✉)

Institute of Mechanics and Printing, Warsaw University of Technology, Narbutta 85, 02-524 Warszawa, Poland

e-mail: marek.pawlikowski@pw.edu.pl

severity of coronary lesions, is calculated as the ratio between the averaged blood flow pressure measured distally to that measured proximally to the stenosis. FFR is obtained invasively by measurement of both pressure values by means of a guiding catheter and a sensor-tipped pressure wire. For some years now non-invasive methods of ischemia diagnosis have been developing. The method of FFR calculation based on computer tomography (FFR-CT) is commonly used. FFR-CT incorporates computational fluid dynamics to estimate the functional data (FFR values) from anatomic images obtained by means of CT coronary angiography. A systematic review of the diagnostic performance of FFR-CT compared to FFR as the reference standard was presented in [9]. The authors reported very high compliance of diagnoses based on FFR-CT with those based on invasive FFR, especially in the cases of patients whose coronary arteries were minimally diseased or normal ($FFR > 0.80$) and the patients qualified for stenting ($FFR < 0.60$). The FFR-CT gave less certainty of diagnosis in the case of patients with FFR between 0.60 and 0.80. The study showed that the diagnostic accuracy of FFR-CT varied across the spectrum of disease. In general, FFR-CT shows a significant correlation with invasive FFR; however, additional studies are required to determine its diagnostic performance [10–13].

Stress cardiovascular magnetic resonance imaging (CMR) is another non-invasive method to diagnose myocardial ischemia. It is also widely used to document ischemia in qualification for coronary revascularization [14]. An attempt to evaluate the agreement of CMR with FFR as the gold standard in assessing the severity of stenoses in IHD has been made by Siastała et al. [15]. The authors analysed 25 consecutive patients who underwent both CMR and FFR to diagnose possible stenosis. They concluded that CMR was clinically useful mostly in patients with stable IHD. Whereas, for patients with a high pretest probability of IHD, CMR method may be applied as a confirmatory test. Recent study shows that CMR seems to be an excellent tool for the assessment of IHD [16]. However, the utilisation of CMR is hampered by several factors, such as claustrophobic and obese patients may not be able to tolerate the examination, patients with implantable ferromagnetic material-made devices should not be examined by means of CMR, relatively high cost compared to invasive FFR method.

It is acknowledged that invasive FFR will remain an important determinant of the treatment indication of IHD. Nevertheless, newer less- and non-invasive techniques are expected to play an increasingly important role in the diagnosis. In our paper, a pilot study in this regard, we present a method of non-invasive FFR estimation based on 3D numerical simulations of blood flow through coronary arteries. It is expected that such simulations will give reliable value of FFR and in future will be utilised in qualification for a surgical procedure. Once the method is fully developed and validated, it can be utilised to assess FFR value in patients with, e.g. implanted an artificial (mechanical) aortic valve (AV). We have not found any studies which undertake the problem of possible FFR value change after an AV implantation. There is some research dealing with FFR estimation after transcatheter aortic valve implantation (TAVI) [17–19]. It has to be underlined that during a TAVI procedure a natural aortic valve is implanted, i.e. pork or beef pericardium on a metallic stent is inserted.

In our study, we aim to assess the difference in FFR values in patients with a mechanical valve implanted. Nowadays, mainly mechanical aortic valves with two leaflets (bileaflet (BIL) AVs) are implanted. However, also studies on AVs with three leaflets (trileaflet (TRI) AVs) are also carried out [20–22]. Analyses of blood flow through BIL and TRI are presented in our previous paper [23]. The analyses are based on numerical simulations performed by means of finite element method (FEM) where boundary conditions play a significant role [24]. A few words regarding this matter are presented in the last section. In the present paper, we estimate a possible change in FFR value in patients who underwent an implantation of BIL valve and a TRI valve [23]. Simulation of blood flow in the coronary arteries in a patient with the natural aortic valve is also carried out. The results of the simulations are compared and analysed.

2 Methods

2.1 Study Design

The main objective of this study was to analyse the effect of mechanical heart valves on coronary artery blood flow. Comparison of flow across BIL, TRI and natural aortic valves (Fig. 1) in a patient with CHD will allow us to estimate the impact of mechanical valve geometry on FFR values. The FFR value measured at coronarography was 83%.

Modelling blood flow through blood vessels, which form a branching structure, requires truncation of the model of this structure. Thus, a problem of proper boundary conditions at the distal ends of the vessels arises. The smaller vessels beyond the truncation point must be substituted by boundary conditions to make the simulations more realistic. In our studies, we defined a combination of flow velocity and pressure at the inlet and outlet. Measurement of blood flow velocity (Doppler ultrasound) was used to determine the boundary conditions. To reflect the physiological blood flow, especially in the region of the sinuses where vortices form, we assumed turbulent blood flow and used the $k-\epsilon$ model to determine its turbulent characteristics. Blood was modelled as an incompressible fluid. We assumed the density $\rho = 1060 \text{ [kg/m}^3\text{]}$

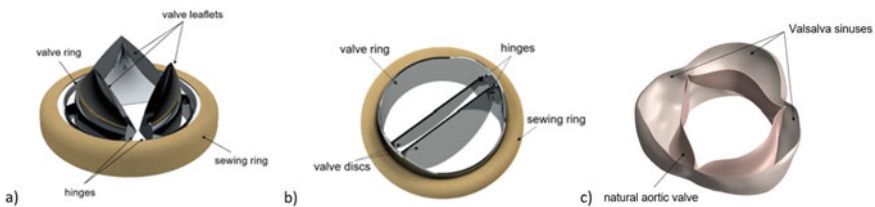


Fig. 1 Aortic valves: **a** TRI, **b** BIL, **c** natural

and viscosity $\mu = 0.0035$ [kg/(m·s)] [25]. The Navier–Stokes equations defined the flow.

2.2 Geometry and Meshing

The geometrical model of blood was generated in Mimics software from CT images of a 50-year-old man with coronary artery stenosis. The CT scan was performed on a 384 Slice Cardiac CT scanner (spatial resolution is 0.24 [mm]). Blood in the coronary arteries is visible on CT images due to the contrast medium added during the coronarography. The model consisted of the aortic root (with Valsalva sinuses) and coronary arteries (Fig. 2). The inner diameter of the ascending aorta is about 30 [mm], the diameter of the inlet is about 23 [mm].

In our study, we considered two types of mechanical valves, i.e. BIL and TRI valves and natural aortic valve. The design of the mechanical valve rings and BIL valve discs was modelled in our previous study [23]. Following the conclusions of our recent study, we modified the shape of the TRI valve leaflets to increase the effective orifice area E_{OA} (Fig. 3). The geometry of the natural valve was modelled based on the anatomical structure of the valve leaflets.

The dynamics of blood circulation were determined using ANSYS 2020 R2 software. The use of the Fluent Flow module allowed the determination of accurate flow

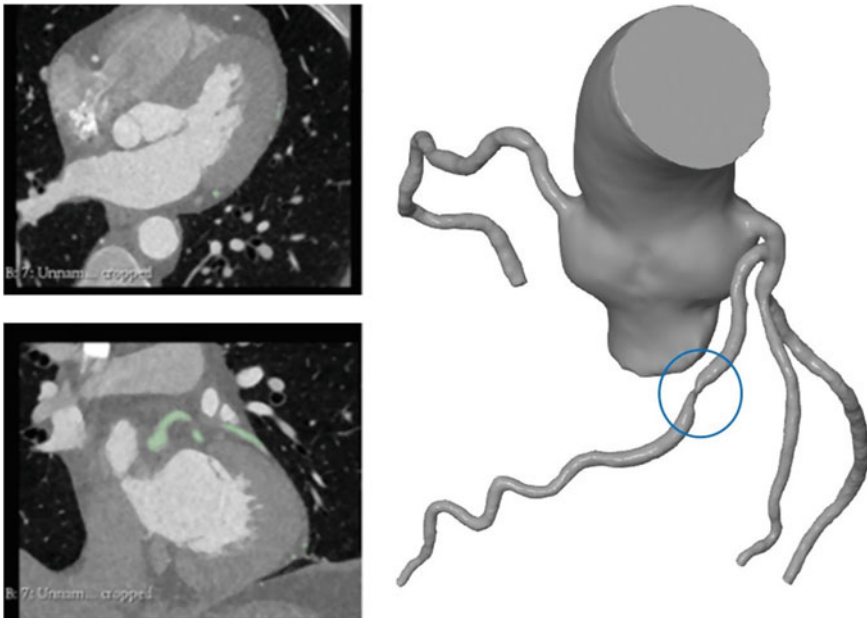


Fig. 2 Model of the whole analysed system

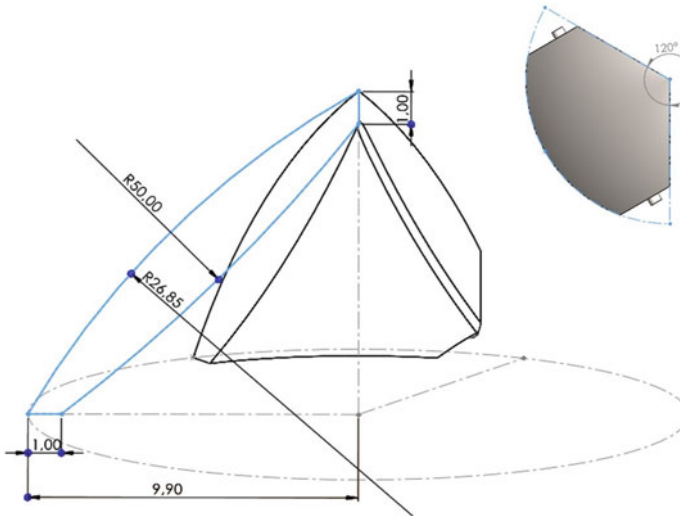


Fig. 3 Shape of the TRI valve leaflet

characteristics. A pressure-based solver was used for the calculations. The numerical model showed the blood model (Fig. 4a) without considering the tissues. The whole blood system was discretised into 2.5 million finite elements. The mesh is made of tetrahedron elements.

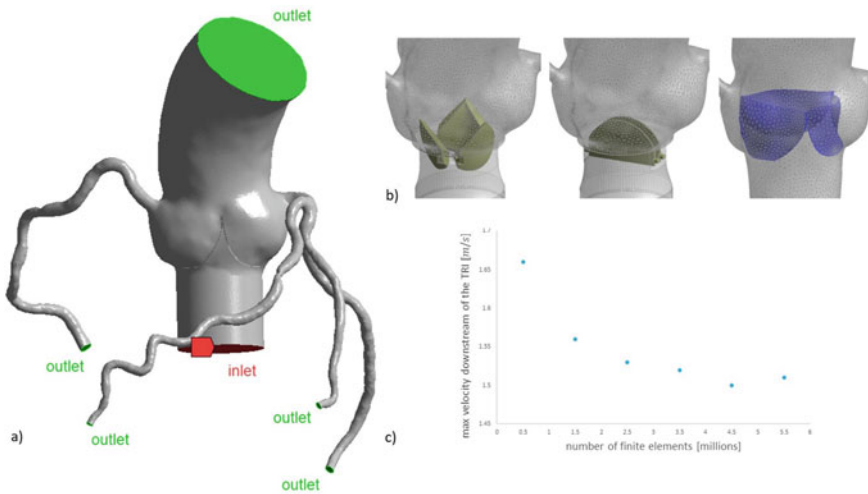


Fig. 4 a Fluid domain with the inlet and outlets, b TRI, BIL (mechanical valves) and natural valve location in numerical model (from left to right), c Influence of the number of the finite elements on maximal velocity downstream of the TRI valve

We confirmed the mesh independence of the flow model solution by comparing the max velocities (Fig. 4c). In addition, the quality of the mesh representing blood was checked. The Orthogonal Quality is about 0.79, and the Skewness is about 0.21. The values obtained indicate a grid of good quality.

Numerical analyses were performed on a workstation with the following parameters: AMD Ryzen 7 3700X 8-Core Processor, 32 GB RAM, 64-bit operation system, and NVIDIA Quadro graphic card.

2.3 Boundary Conditions

The correlation of the flow velocity and valve opening time was determined by Doppler ultrasound and described by Eqs. (1)-(3) [23]. The length of one cycle is 0.8 [s]. Numerical measurement of FFR was performed during the hyperemia (for $t = 0.29$ [s]).

for $t \in < 0; 0.36$ s)

$$v = 10259.13 \cdot t^6 - 13602.92 \cdot t^5 + 6827.23 \cdot t^4 - 1500.76 \cdot t^3 + 90.61 \cdot t^2 + 9.54 \cdot t \quad (1)$$

for $t \in < 0.36; 0.38$ s)

$$v = 2.5 \cdot t - 0.95 \quad (2)$$

for $t \in < 0.38; 0.8$ s)

$$v = 0 \quad (3)$$

Flow velocity values were determined at the inlet, which was defined at the aortic inlet. At the outlet of the coronary arteries, a pressure of 1.3 [kPa] was defined, allowing for consideration of vascular resistance and normal myocardial perfusion.

Figure 4a illustrates the boundary conditions, and Fig. 4b shows a scheme of valve locations in the model.

3 Results

The FFR is defined as the ratio of mean pressure measured distally behind the stenosis location (P_d) to mean pressure measured proximally (P_a) during hyperemia Eq. (4). The $FFR < 0.8$ determines surgical treatment.

$$FFR = \frac{P_d}{P_a} \tag{4}$$

Using data from the results of pressure distribution, the FFR ratio for the natural valve, BIL valve and TRI valve was calculated and compared with the results of coronarography (Table 1). The pressure (P_d and P_a) was calculated at a distance of five stenosis diameters from the maximum coronary artery stenosis as it is measured during the examination.

In Figs. 5 and 6, the flow velocity magnitude changes in the aortic root and ascending aorta, and the velocity distribution are shown, respectively.

In Fig. 7, the geometry of the aortic root is presented. The Valsalva sinuses can be clearly seen. In geometrical modelling of the aorta and coronary arteries it is crucial to model accurately the sinuses geometry as it significantly influences the results of blood flow simulation. In addition, correct location of the sinuses in the model determines the orientation of the mechanical valve placement. During building the assembly models of the aorta and mechanical valves we paid special attention to the leaflet position in terms of a possible obstruction of blood flow into coronary arteries.

We also calculated the effective orifice area E_{OA} and geometric flow area of the fluid through the valves (Table 2). Determination of E_{OA} allows assessment of the pressure gradient through the valve. In this way, it evaluates whether the flow area

Table 1 FFR ratio

	FFR [%]
Coronarography	83
Natural valve	82
BIL valve	77
TRI valve	75

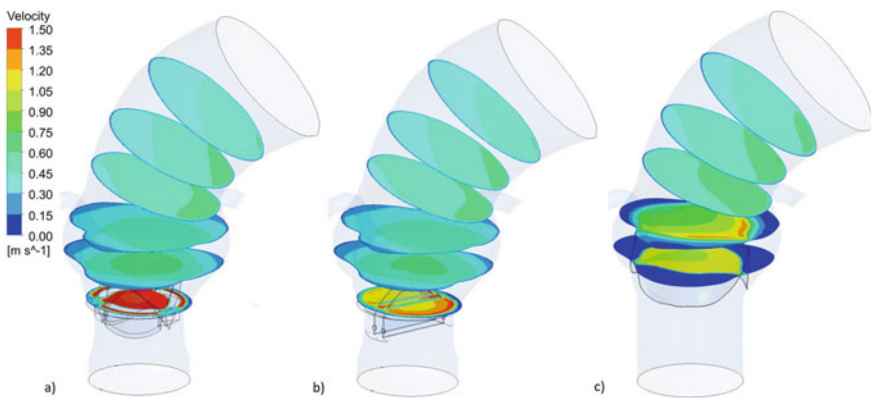


Fig. 5 Flow velocity magnitude change in the aortic root and ascending aorta for the valve: **a** TRI, **b** BIL, **c** natural

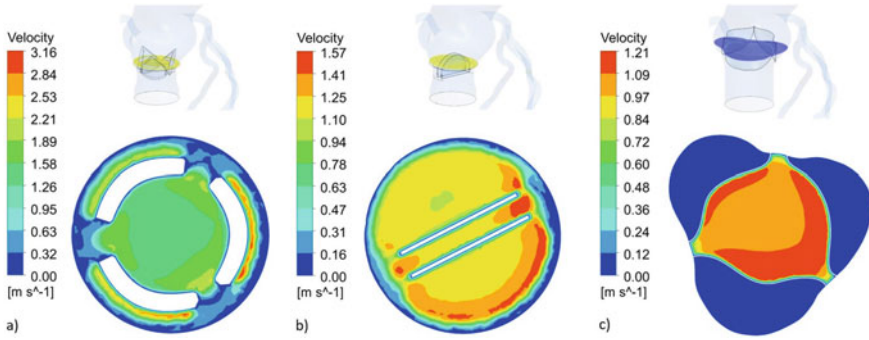


Fig. 6 Velocity magnitude distribution for the valve: **a** TRI, **b** BIL, **c** natural

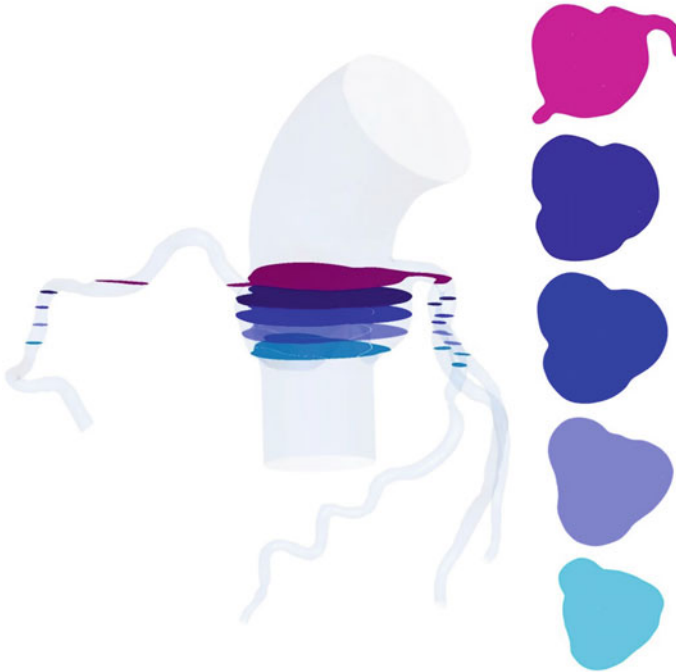


Fig. 7 Patient-specific aortic root geometry

is large enough to prevent the pressure gradient from increasing, which can lead to heart failure. To calculate E_{OA} , we used the corrected Gorlin formula in the form [26]:

$$E_{OA} = \frac{Q}{51.6 \sqrt{\frac{\Delta p}{\rho}}} \quad (5)$$

Table 2 E_{OA} and geometric valves flow area

	E_{OA}	Geometric flow area [cm ²]
Natural valve	2.85	3.74
BIL valve	1.53	2.88
TRI valve	0.73	1.61

where Q is the volume flow rate in [mL/s], Δp is the average pressure difference through the valve in [mmHg], and ρ is the blood density in [g/cm³]. The number 51.6 is the gravitational acceleration constant.

The calculations were based on $Q = 110$ [mL/s] (the value obtained from the study for the analysed patient) and $\rho = 1.06$ [g/cm³].

4 Discussion

Modern high-resolution CT enables obtaining exact images converted into precise 3D models of blood. These models can be used in simulations of blood flow. The value of the FFR ratio (Table 1) for the natural valve predicted in our numerical simulation (82%) is near to the FFR value from coronarography (83%). The obtained results confirm the validity of the simulations. Since the predicted and measured FFR values for natural valve are almost the same, we hypothesise that the numerical model is accurate enough to reliably predict the FFR values for the artificial valves. The FFR values for BIL and TRI mechanical valves are 77 and 75%. The difference in FFR values for the natural valve compared to the BIL and TRI valves is 5 and 7%, accordingly. The differences in the results may be due to the smaller E_{OA} of the mechanical valves (Table 2). Although the E_{OA} for the TRI valve (0.73 [cm²]) is smaller than that for the BIL valve (1.53 [cm²]), the FFR value differs slightly. This is probably due to the shape of the TRI valve leaflets, which point towards the sinuses of Valsalva at the maximum opening and allow unobstructed blood flow into the coronary arteries.

Studies suggest that geometric parameters of the coronary artery are essential in the final haemodynamic results of the simulations. This issue is critical because coronary branches' number, length, irregularity, and given boundary conditions at the ends influence the pressure value behind the stenosis. Defining distal boundary conditions is particularly challenging, as circulatory conditions in the coronary microcirculation are heterogeneous in health and disease. Consequently, their underestimation or omission may distort the FFR ratio determined by us. The values of pressure in a coronary artery, and consequently those of FFR, strongly depend on boundary conditions, especially those defined in the truncated ends of the arteries at the outlets [27]. Identification of the outlet boundary conditions is not trivial as measurement of reliable blood flow, pressure, or resistance at each outlet is practically impossible [28]. However, there are methods which make it possible to estimate the outlet resistance according to myocardial perfusion territory. One of the newest approaches

in the outlet boundary conditions definition is reported in [29]. The authors developed a personalised CT-based coronary blood flow model to estimate coronary outlet resistance and distributed outlet coronary blood flow based on myocardial perfusion territory. Although their method seems to be reliable, they stated that it still requires further validation.

Our study considered patient-specific coronary artery geometry (Fig. 2). Carvalho et al. [30] use an idealised geometry, which may impact fluid dynamics. Researchers use different blood viscosity models and flow conditions to study flow. It is generally accepted that blood behaves as a Newtonian fluid in large coronary vessels [31, 32]. However, it should be noted that in areas of constriction, due to the ability of red blood cells to form aggregates, blood should be defined as a non-Newtonian fluid [33, 34]. Only a few studies have evaluated the impact of different inlet and outlet boundary conditions. Researchers use velocity, pressure or flow rate combinations at the inlet while at the outlet constant pressure outlet, Windkessel model or zero gauge pressure [30, 31, 35]. In our study, we assumed velocity at the inlet, which was determined by Doppler ultrasound, and pressure at the outlet allowing for consideration of vascular resistance (Fig. 4a). In future studies, we will focus on analysing the effect of preset boundary conditions on the corresponding behaviour of blood flow in coronary arteries. There is no substantial evidence that it is necessary to reflect the movement of the vessel wall to calculate FFR. Typically, rigid wall conditions are used [32, 33]. Our future studies will also focus on examining the effect of considering coronary artery walls on flow and FFR.

Our model takes into account the sinuses of Valsalva, which have individually defined shapes and dimensions. Consideration of the real geometry allows for accurate results. De Tulio et al. conducted numerical simulations of blood flow after a mechanical aortic valve and studied the influence of the aortic root geometry on blood behaviour in the region of sinuses [36]. They considered three models, i.e. three sinuses, one sinus in the form of an axisymmetric bulb, and a simple aorta without sinuses. Their results indicate that the aortic root's geometry only marginally affects the kinematic features of blood flow downstream of a mechanical valve. Only minor changes in velocities were observed. However, differences in the dynamics of blood flow resulting from the aortic root geometry are noticeable. The authors of [37] observed the formation of vortices in the region of the sinuses. Their numerical results show a presence of negative velocities that they interpreted as blood recirculation in the sinuses. However, researchers do not consider coronary arteries, which have their origins in the sinuses and may significantly affect fluid dynamics in the aortic root. In consequence, the wall boundary condition is imposed on the inner surfaces of the sinuses. This is a factor that benefits vortex formation in the region. In [36], the authors modelled the aortic root geometry with coronary arteries truncated at a close distance from the aorta and defined boundary conditions that “are limiting in that, in general, they do not accurately replicate vascular impedance of the downstream vasculature”. This means that they did not consider the inertia of the fluid of all the neglected parts of the vascular network, nor did they consider the compliance of the arteries. The primary characteristics of coronary flow were analysed by Querzoli et al. [38]. They concluded that 75% of the flow in coronary arteries occurs during

diastole. During systole, no distinct effects were observed, except for a secondary vortex region located at the inlet of the coronary vessel. In future studies, we will focus on comparing the behaviour of blood in systole and diastole.

The flow distribution in the ascending aorta is determined by the curvature of the aortic arch (Fig. 5). Maximum flow velocities occur in the TRI valve because a gap between the leaflet and the valve ring remains during maximal leaflet opening (Figs. 5 and 6a). Analysis of fluid behaviour indicates that implanting the valve before the aortic root does not cause vortices in the sinuses of Valsalva and reduces turbulent flow. However, this may have a negative effect on the closure of the valve leaflets. Analysis of Fig. 6 allows us to note the impact of the non-idealised shape of the sinuses on flow. The patient-specific aortic root geometry shows in Fig. 7. There are higher flow velocities in the sinus where the left coronary artery is located, 3.16 [m/s] for TRI, 1.57 [m/s] for BIL and 1.21 [m/s] for the natural valve (Fig. 6).

The study determined the effect of blood pressure gradient in flow across mechanical (TRI and BIL) and natural aortic valves on the fractional coronary flow reserve (FFR) value. Due to their geometry and location, mechanical heart valves have a smaller flow area, so there is a change in the pressure gradient upstream and downstream of the valve. It is worth analysing the location of the implanted artificial heart valve and its effect on the pressure change and optimising the mechanical valve's shape.

References

1. Fossan, F.E., Sturdy, J., Muller, L.O., et al.: Uncertainty quantification and sensitivity analysis for computational FFR estimation in stable coronary artery disease. *Cardiovasc. Eng. Technol.* **9**(4), 597–622 (2018)
2. Knuuti, J., Wijns, W., Saraste, A., et al.: 2019 ESC guidelines for the diagnosis and management of chronic coronary syndromes. *Eur. Heart J.* **41**, 407–477 (2020)
3. Rezende, P.C., Scudeler, T.L., Alves da Costa, L.M., et al.: Conservative strategy for treatment of stable coronary artery disease. *World J. Clin. Cases* **3**, 163–170 (2015)
4. Perera, D., Clayton, T., O’Kane, P.D., et al.: Percutaneous revascularization for ischemic left ventricular dysfunction. *N. Engl. J. Med.* **387**, 1351–1360 (2022)
5. Bojar, R.M.: Cardiovascular management. In: *Manual of Perioperative Care in Adult Cardiac Surgery*. Wiley. ISBN 978-1-119-58255-7 (2021)
6. Li, M., Zhou, T., Yang, L.-F., et al.: Diagnostic accuracy of myocardial magnetic resonance perfusion to diagnose ischemic stenosis with fractional flow reserve as reference: systematic review and meta-analysis. *JACC Cardiovasc. Imaging* **7**, 1099–1105 (2014)
7. Yang, Z., Zheng, H., Zhou, T., et al.: Diagnostic performance of myocardial perfusion imaging with SPECT, CT and MRI compared to fractional flow reserve as reference standard. *Int. J. Cardiol.* **190**, 103–105 (2015)
8. Qayyum, A., Kastrup, J.: Measuring myocardial perfusion: the role of PET, MRI and CT. *Clin. Radiol.* **70**, 576–584 (2015)
9. Cook, C.M., Petraco, R., Shun-Shin, M.J., et al.: Diagnostic accuracy of computed tomography-derived fractional flow reserve. A systematic review. *JAMA Cardiol.* **2**(11), 803–810 (2017)
10. Sonck, J., Nagumo, S., Norgaard, B.L., et al.: Clinical validation of a virtual planner for coronary interventions based on coronary CT angiography. *JACC Cardiovasc. Imaging* **15**, 1242–1255 (2022)

11. Serruys, P.W., Hara, H., Garg, S., et al.: Coronary computed tomographic angiography for complete assessment of coronary artery disease. *J. Am. Coll. Cardiol.* **78**, 713–736 (2021)
12. Tanigaki, T., Emori, H., Kawase, Y., et al.: QFR versus FFR derived from computed tomography for functional assessment of coronary artery stenosis. *JACC Cardiovasc. Interv.* **12**, 2050–2059 (2019)
13. Peper, J., Becker, L.M., van den Berg, H., et al.: Diagnostic performance of CCTA and CT-FFR for the detection of CAD in TAVR work-up. *JACC Cardiovasc. Interv.* **15**, 1140–1149 (2022)
14. Costa, M.A., Shoemaker, S., Futamatsu, H., et al.: Quantitative magnetic resonance perfusion imaging detects anatomic and physiologic coronary artery disease as measured by coronary angiography and fractional flow reserve. *J. Am. Coll. Cardiol.* **50**, 514–522 (2007)
15. Siastala, P., Kądziela, J., Małek, Ł.A., et al.: Do we need invasive confirmation of cardiac magnetic resonance results? *Adv. Interv. Cardiol.* **13**(1), 26–31 (2017)
16. Patel, A.R., Salerno, M., Kwong, R.Y., et al.: Stress cardiac magnetic resonance myocardial perfusion imaging: JACC review topic of the week. *J. Am. Coll. Cardiol.* **78**, 1655–1668 (2021)
17. Scarsini, R., Lunardi, M., Venturi, G., et al.: Long-term variations of FFR and iFR after transcatheter aortic valve implantation. *Int. J. Cardiol.* **317**, 37–41 (2020)
18. Scarsini, R., Pesarini, G., Lunardi, M., et al.: Observations from a real-time, iFR-FFR “hybrid approach” in patients with severe aortic stenosis and coronary artery disease undergoing TAVI. *Cardiovasc. Revasc. Med.* **19**, 355–359 (2018)
19. Ahmad, Y., Götberg, M., Cook, C., et al.: Coronary hemodynamics in patients with severe aortic stenosis and coronary artery disease undergoing transcatheter aortic valve replacement: implications for clinical indices of coronary stenosis severity. *JACC Cardiovasc. Interv.* **11**, 2019–2031 (2018)
20. Nowak, M., Divo, E., Adamczyk, W.P.: Fluid-structure interaction methods for the progressive anatomical and artificial aortic valve stenosis. *Int. J. Mech. Sci.* **227**, 1–20 (2022)
21. Zhou, H., Wu, L., Wu, Q.: Structural stability of novel composite heart valve prostheses—fatigue and wear performance. *Biomed. Pharmacother.* **136**, 1–8 (2021)
22. Cavallo, A., Gasparotti, E., Losi, P., et al.: Fabrication and in-vitro characterization of a polymeric aortic valve for minimally invasive valve replacement. *J. Mech. Behav. Biomed. Mater.* **115**, 1–9 (2021)
23. Pawlikowski, M., Nieroda, A.: Comparative analyses of blood flow through mechanical trileaflet and bileaflet aortic valves. *Acta Bioeng. Biomech.* **24**, 141–152 (2022)
24. Vignon-Clementel, I.E., Figueroa, C.A., Jansen, K.E., et al.: Outflow boundary conditions for 3D simulations of non-periodic blood flow and pressure fields in deformable arteries. *Comput. Methods Biomech. Biomed. Eng.* **13**, 625–640 (2010)
25. Ali, A., Kazmi, R.: High performance simulation of blood flow pattern and transportation of magnetic nanoparticles in capillaries. *Intell. Technol. Appl.* **1198**, 222–236 (2020)
26. Hui, S., Mahmood, F., Matyal, R.: Aortic valve area-technical communication: continuity and Gorlin equations revisited. *J. Cardiothorac. Vasc. Anesth.* **32**(6), 2599–2606 (2018)
27. Taylor, C.A., Figueroa, C.: Patient-specific modeling of cardiovascular mechanics. *Ann. Rev. Biomed. Eng.* **11**, 109–134 (2009)
28. Morris, P.D., van de Vosse, F.N., Lawford, P.V., et al.: “Virtual”(computed) fractional flow reserve: current challenges and limitations. *JACC: Cardiovasc. Interv.* **8**(8), 1009–1017 (2015)
29. Xue, X., Liu, X., Gao, Z., et al.: Personalized coronary blood flow model based on CT perfusion to non-invasively calculate fractional flow reserve. *Comput. Methods Appl. Mech. Eng.* **404**, 115789 (2023)
30. Carvalho, V., Rodrigues, N., Ribeiro, R., et al.: Hemodynamic study in 3D printed stenotic coronary artery models: experimental validation and transient simulation. *Comput. Methods Biomech. Biomed. Eng.* **24**(6), 623–636 (2020)
31. Lo, E.W.C., Menezes, L.J., Torii, R.: Impact of inflow boundary conditions on the calculation of CT-based FFR. *Fluids* **4**(2), 60 (2019)
32. Carvalho, V., Rodrigues, N., Ribeiro, R., et al.: 3D printed biomodels for flow visualization in stenotic vessels: an experimental and numerical study. *Micromachines* **11**(6), 549 (2020)

33. Kashyap, V., Arora, B.B., Bhattacharjee, S.: A computational study of branch-wise curvature in idealized coronary artery bifurcations. *Appl. Eng. Sci.* **4**, 100027 (2020)
34. Pandey, R., Kumar, M., Srivastav, V.K.: Numerical computation of blood hemodynamic through constricted human left coronary artery: pulsatile simulations. *Comput. Methods Program. Biomed.* **197**, 105661 (2020)
35. Zhao, Y., Ping, J., Yu, X.: Fractional flow reserve-based 4D hemodynamic simulation of time-resolved blood flow in left anterior descending coronary artery. *Clin. Biomech.* **70**, 164–169 (2019)
36. de Tullio, M.D., Pedrizzetti, G., Verzicco, R.: On the effect of aortic root geometry on the coronary entry-flow after a bileaflet mechanical heart valve implant: a numerical study. *Acta Mech.* **216**(1), 147–156 (2011)
37. Belkhiri, K., Boumeddane, B.: A Cartesian grid generation technique for 2-D non-Newtonian blood flow through a bileaflet mechanical heart valve. *Int. J. Comput. Methods Eng.* **22**(4), 297–315 (2021)
38. Querzoli, G., Fortini, S., Espa, S., et al.: A laboratory model of the aortic root flow including the coronary arteries. *Exp. Fluids* **57**(8), 1–9 (2016)